Journal of *Marine Science and Engineering*

MDPI

Article

A Composite Super-Twisting Sliding Mode Approach for Platform Motion Suppression and Power Regulation of Floating Offshore Wind Turbine

Wenxiang Yang [1], Yaozhen Han [1,*], Ronglin Ma [2], Mingdong Hou [1] and Guang Yang [1]

[1] School of Information Science and Electrical Engineering, Shandong Jiaotong University, Jinan 250357, China; ywxxueshu@163.com (W.Y.); houmingdong@sdjtu.edu.cn (M.H.); yangguang@sdjtu.edu.cn (G.Y.)
[2] School of International Education, Shandong Jiaotong University, Jinan 250357, China; maronglin@sdjut.edu.cn
* Correspondence: hanyz@sdjtu.edu.cn

Abstract: The floating platform motion of an offshore wind turbine system can exacerbate output power fluctuations and increase fatigue loads. This paper proposes a new scheme based on a fast second-order sliding mode (SOSM) control and an adaptive super-twisting extended state observer to suppress the platform motion and power fluctuation. Firstly, an affine nonlinear model of the floating wind turbine pitch system is constructed. Then, a fast SOSM pitch control law is adopted to adjust the blade pitch angle, and a new adaptive super-twisting extended state observer is constructed to achieve total disturbance observation. Finally, simulations are conducted under two cases of wind and wave conditions based on FAST (fatigue, aerodynamics, structures, and turbulence) and MATLAB/Simulink. Compared with the traditional proportional integral (PI) control scheme and standard super-twisting control scheme, the platform roll under the proposed scheme is reduced by 13% and 4%, and pitch is reduced by 16% and 3% in Case 1. Correspondingly, the roll is reduced by 9% and 15%, and pitch is reduced by 7% and 1% in Case 2. For the tower top pitch and yaw moment, load reductions of 7% and 3% or more are achievable compared with those under the PI control scheme. It is indicated that the proposed scheme is more effective in suppressing floating platform motion, stabilizing output power of the wind turbine system, and reducing tower loads.

Keywords: floating offshore wind turbine; composite super-twisting sliding mode; platform motion; fatigue load; output power

Citation: Yang, W.; Han, Y.; Ma, R.; Hou, M.; Yang, G. A Composite Super-Twisting Sliding Mode Approach for Platform Motion Suppression and Power Regulation of Floating Offshore Wind Turbine. *J. Mar. Sci. Eng.* **2023**, *11*, 2318. https://doi.org/10.3390/jmse11122318

Academic Editors: Kostas Belibassakis, Eugen Rusu and George Lavidas

Received: 10 November 2023
Revised: 3 December 2023
Accepted: 5 December 2023
Published: 7 December 2023

1. Introduction

Wind energy utilization is an important measure to achieve the goal of carbon neutrality, and solve the energy crisis and environmental pollution [1]. The development and utilization of onshore wind energy has gradually moved towards industrialization and large-scale direction. However, onshore wind farms are severely limited by resource regions, and face visual and noise impacts [2]. Offshore wind power has become the key development direction for countries around the world due to its advantages of saving land, stable operation, and being close to load center of the grid [3,4]. According to the different types of platform foundation, offshore wind turbines are divided into fixed and deep-sea floating types [5]. With the gradual saturation of the development intensity of wind power resources in the intertidal zone and offshore areas, and the growing demand for environmental protection in coastal areas, it will be an inevitable trend for offshore wind power to move from the intertidal zone and offshore to the deep sea. In recent years, the floating type suitable for the deep sea has attracted wide attention [6].

The platform foundation of a floating offshore wind turbine (FOWT) is easily excited by wind and wave loads, leading to more platform motion, which makes the wind turbine withstand more fatigue loads [6,7]. Additionally, the coupling between blade pitch control

system and platform dynamics aggravates the platform motion when wind speed is higher than the rated value [8,9]. Repeated platform motion does not only damage mechanical components and reduce the service life of the FOWT, but also cause fluctuations in power output and deteriorate power generation performance. Although the control methods for onshore wind turbines are becoming increasingly mature, they cannot be directly applied for the FOWT. There are relatively few controllable degrees of freedom. The goals of load suppression and power regulation are mutually restrictive. It is particularly important to design a new control scheme to reduce platform motion, suppress fatigue loads, and stabilize power generation.

The methods for inhibiting platform motion and reducing load are currently mainly divided into two categories. One is to use structural-vibration-control-tuned mass dampers (TMDs) on the FOWT to increase control freedom. TMDs are used for passive control to limit nacelle or platform motion. Lackner et al. [10] developed an advanced modeling tool to determine optimal parameters for the TMD system, thereby improving the structural response of offshore wind turbines. Based on this, Stewart et al. [11] adopted a genetic algorithm to find the global optimization design of TMDs, determining the TMD parameters and conducting sensitivity analysis in order to reduce fatigue damage to the tower. Sarkar et al. [12] conducted research on passive tuned mass-damper-inerter (TMDI); compared with classical TMDs, TMDIs exhibit stronger vibration control ability. However, the complexity of a TMD system is related to the number of degrees of freedom that need to be controlled along each axis. As more degrees of freedom are added, the TMD system becomes more complex and requires additional installation space and costs [13]. Another method is to adjust the blade pitch angle of the FOWT based on some advanced control algorithms such as PI control [14], predictive control [15], state-space feedback control [16] and linear quadratic regulator [17,18]. These control methods are based on linearized models. Yet, as the wind energy conversion system is a set of typical complex dynamic systems, and there are wind and wave disturbances. The effectiveness of these linear model controllers may diminish with changes in the operating point. Therefore, it is of great importance to improve the system's robustness.

Sliding mode control (SMC) has strong robustness to disturbances and unmodeled dynamics, and can overcome system uncertainty. SMC studies for the onshore wind power system have been gradually carried out [19,20]. However, FOWT control is more complex, and multiple cooperative objectives need to be achieved through pitch control. Meanwhile, severe chattering in traditional first-order SMC can negatively impact the pitch actuator. Shah et al. [21] proposed a scheme combining terminal sliding mode with a translational oscillator for a barge-type FOWT. Yet, the chattering phenomenon induced by the first-order SMC is prone to damage the pitch actuator. High-order SMC, which has become a research focus of the sliding mode algorithm in recent years, achieves chattering suppression by hiding high-frequency switching in the high-order differential of the control variable [22]. The super-twisting second-order SMC algorithm is a special form of high-order SMC algorithms. It does not require known differential information of sliding mode variables and can achieve continuous control [23]. Recently, Zhang et al. [24–26] attempted to apply second-order SMC to the FOWT control, and it has played a positive role in regulating output power and stabilizing the floating platform. However, their design scheme is based on the linear model of a certain equilibrium point which describes the system as a black box, and SMC is directly executed. This approach ignores wind/wave description and the known parts of the system. This leads to an excessive SMC effect, which worsens the damage to the pitch actuator. Our team has also carried out a preliminary study on pitch control via second-order SMC [27].

In fact, the FOWT is affected by external disturbances such as wind, wave, and current, as well as internal parameter perturbations. However, SMC has the disadvantage of being insensitive to unmatched uncertainties. Moreover, the control gains of the sliding mode controller are usually chosen conservatively to obtain good performance in the presence of disturbances. To further alleviate the well-known chattering problem and maintain nominal control of SMC in the presence of both matched and nonmatched disturbances, some schemes combining the disturbance observer with SMC have been presented [28–32]. However, the FOWT faces both matched and unmatched disturbances. Whether based on a model or not, existing observers cannot simultaneously estimate these disturbances. Moreover, the observer gain can only be monotonically increased, which is not truly adaptive.

Hence, this paper proposes a new composite pitch control scheme for load suppression and power regulation of the FOWT. The proposed scheme is verified via FAST and MATLAB/Simulink. Furthermore, power spectral density (PSD) analysis of the FOWT output power and floating platform motion is conducted. The novelty mainly includes the following: (1) A new scheme based on a fast SOSM control and an adaptive super-twisting extended state observer is proposed to suppress the platform motion and power fluctuation of FOWT. The controller combines the advantages of the linear algorithm and the super-twisting control (STC) algorithm to handle disturbances near and far from the origin. (2) For the nonlinear affine uncertain system with pitch angle and speed, an extended state observer is designed based on an adaptive super-twisting algorithm to observe the total disturbances. The proposed control scheme can be more effective in restraining floating platform motion, stabilizing generator output power and restraining tower load, and has stronger adaptability to the environment than PI and the standard super-twisting control scheme.

This paper is organized as follows. Section 2 introduces a 5 MW offshore wind turbine model which utilizes a barge-type floating platform. Section 3 provides a detailed analysis of the proposed control scheme. Section 4 describes the simulation environment and simulation settings, and discuss the effectiveness of the proposed scheme on a 5 MW barge-type FOWT. Finally, Section 5 summarizes the conclusions of our work.

Table 1 shows the acronyms used within this paper for a better understanding.

Table 1. Acronyms used.

SOSM	second-order sliding mode
PI	proportional integral
FOWT	floating offshore wind turbine
TMD	tuned mass dampers
TMDI	tuned mass-damper-inerter
SMC	sliding mode control
PSD	power spectral density
STC	super-twisting control
CSTSM	composite super-twisting sliding mode
SSTSM	standard super-twisting sliding mode
DEL	damage equivalent load
RMS	root mean square

2. FOWT Model

This study's object is the NREL (National Renewable Energy Laboratory) 5 MW wind turbine, shown in Figure 1, with the ITI Energy barge-type floating platform [33]. The platform is stabilized by a mooring system which employs the catenary type with 8 anchor chains rectangular mooring method.

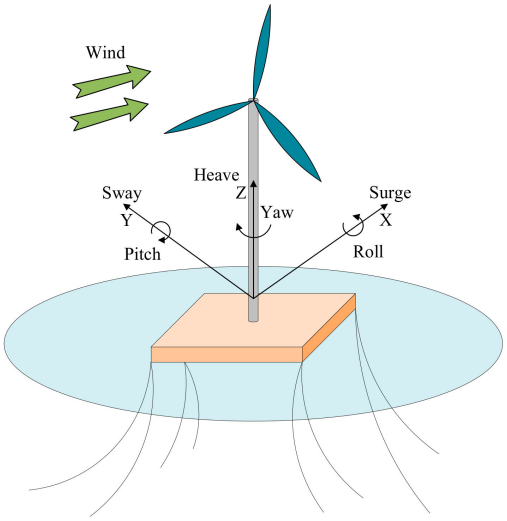

Figure 1. Barge-type FOWT model.

The mechanical dynamics relationship of the wind turbine is as follows [34,35]:

$$\dot{\omega} = -\frac{B}{J}\omega + \frac{T}{J} - \frac{N}{J}T_{\mathrm{g}} \tag{1}$$

in which B is the viscous friction coefficient, T_g is generator torque, J is the inertia coefficient, N is the gearbox ratio, ω is the rotor angular velocity of the wind turbine, and T is rotor torque. Their relationship is

$$\begin{cases} \omega = \frac{P\lambda}{KR\omega C_P(\lambda,\beta)v^2} \\ T = \frac{KRC_P(\lambda,\beta)v^2}{\lambda} \\ K = \frac{1}{2}\pi\rho R^2 \end{cases} \tag{2}$$

where P is mechanical power captured by wind turbine, ρ is air density, R is rotor radius, λ is tip speed ratio, v is incoming wind speed, β is pitch angle, and $C_p(\lambda,\beta)$ is power capture coefficient of wind turbine, which can be simplified as

$$\overline{C}_P(\lambda,\beta) = \overline{G}_5(\overline{b}_1\lambda + \overline{b}_2)[h_1(\lambda) - \beta \cdot h_2(\lambda)] + d_1(\lambda,\beta) \tag{3}$$

where $h_1(\lambda) = \overline{G}_1/\lambda + \overline{G}_3$, $h_2(\lambda) = 0.08\overline{G}_1/\lambda^2 - \overline{G}_2$, $d_1(\lambda,\beta)$ is the error after simplification, and the coefficient $\overline{G}_i(i = 1,2,\ldots,5)$ is the nominal value of $G_i(i = 1,2,\ldots,5)$.

There are errors between the actual and nominal values of B and J. These bounded unknown values can be expressed as

$$\begin{cases} J = \overline{J} + \Delta J & |\Delta J| \le d_{\mathrm{J}} \\ B = \overline{B} + \Delta B & |\Delta B| \le d_{\mathrm{B}} \end{cases} \tag{4}$$

where $\overline{B}$ and $\overline{J}$ are nominal values, ΔB and ΔJ are uncertainties, and d_B and d_J are the unknown upper bound.

In summary, the wind turbine model can be described as

$$\begin{cases} \dot{\omega} = \frac{KRv^2}{\overline{J}\lambda}\overline{G}_5(\overline{b}_1\lambda + \overline{b}_2)[h_1(\lambda) - \beta h_2(\lambda)] + d(\lambda,\beta,v,\omega) \\ d(\lambda,\beta,v,\omega) = -\frac{N}{\overline{J}}\frac{\hat{P}}{\omega} + \frac{KRv^2}{\overline{J}\lambda} \cdot d_1(\lambda,\beta) - \frac{\overline{B}}{\overline{J}}\omega + d_2(\lambda,\beta,v,\omega) \end{cases} \tag{5}$$

where $d_2(\lambda,\beta,v,\omega)$ is caused by system parameter uncertainty and wave disturbance. Considering the physical limitations of the wind turbine, $d(\lambda,\beta,v,\omega)$ is bounded and unknown.

3. Control Scheme

To stabilize output power, reduce platform motion, lower fatigue load, and realize robust control of the FOWT, this paper proposes a new collective pitch control scheme combining the sliding mode controller and observer with algorithm simplicity consideration. A fast super-twisting SOSM pitch controller is designed to adjust the pitch angle, and an adaptive super-twisting extended state observer is constructed to observe and compensate for the total system disturbances.

The sliding mode function is designed as

$$\sigma = \omega - \omega^* + c\int_0^t (\omega - \omega^*)d\tau \tag{6}$$

where c is a positive parameter, and ω^* is the rated rotor angular velocity with platform displacement consideration [36], which is represented as

$$\omega^* = \omega_r - k\dot{\theta} \tag{7}$$

where ω_r is the rated rotor angular velocity without platform displacement consideration, $\dot{\theta}$ is the platform pitch angular velocity, and k is the user-defined positive parameter. When the wind turbine tilts upwind, more energy can be obtained from wind by increasing the rated rotor angular velocity ω^*; thereby, the platform motion is suppressed. When the wind turbine pitches in the direction of wind, less energy is extracted due to reducing ω^*, and suppressing its movement again. Thus, the effect of suppressing platform motion is achieved by tracking the rated rotor angular velocity ω^* through the actual rotor angular velocity.

By substituting Equation (5) into Equation (6), it can be deduced that

$$\begin{aligned}
\dot{\sigma} &= \dot{\omega} - \dot{\omega}^* + c(\omega - \omega^*) \\
&= \frac{KRv^2}{\bar{J}\lambda}\bar{G}_5(\bar{b}_1\lambda + \bar{b}_2)[h_1(\lambda) - \beta h_2(\lambda)] + d(\lambda, \beta, v, \omega) - \dot{\omega}^* + c(\omega - \omega^*) \\
&= \underbrace{\frac{KRv^2}{\bar{J}\lambda}\bar{G}_5(\bar{b}_1\lambda + \bar{b}_2)\cdot h_1(\lambda) + c(\omega - \omega^*) - \dot{\omega}^*}_{\bar{f}(\lambda,\beta,v,\omega)} + \underbrace{(-1)}_{g}\cdot\underbrace{\beta}_{u} \\
&+ \underbrace{[-\frac{KRv^2}{\bar{J}\lambda}\bar{G}_5(\bar{b}_1\lambda + \bar{b}_2)\cdot h_2(\lambda) + 1]\beta + d(\lambda, \beta, v, \omega)}_{\Delta} \\
&= \bar{f} + g\cdot u + \Delta,\ |\dot{\Delta}| \le N
\end{aligned} \tag{8}$$

where $\bar{f}$ is the nominal value, Δ is the total system disturbances, and N is the unknown upper bound of the total disturbance derivative.

The control input is designed as

$$u = \frac{1}{g}(-\bar{f} + u_s) \tag{9}$$

where u_s is the auxiliary control. Then, Equation (8) is converted as

$$\dot{\sigma} = u_s + \Delta \tag{10}$$

For Equation (10), standard super-twisting second-order SMC can be applied.

$$\begin{cases} u_s = -k_1|\sigma|^{1/2}sign(\sigma) + u_1 \\ u_1 = -k_3 sign(\sigma) \end{cases} \tag{11}$$

where k_1 and k_3 are control gains. SOSM with respect to σ can be established by selecting parameters $k_1 = 1.5\sqrt{N}$ and $k_2 = 1.1N$ [37].

The total disturbances value Δ is unknown but its derivative has an upper bound N. If a disturbance observer is used to observe the disturbances in real time, the controller gains can be effectively lowered and the disturbances' impact on the FOWT can be reduced. To define this, $\hat{\Delta}$ is the observed value of Δ and $\widetilde{\Delta}$ is the observation error, $\Delta = \hat{\Delta} + \widetilde{\Delta}$. Then, Equation (8) becomes

$$\dot{\sigma} = \overline{f} + g \cdot u + \hat{\Delta} + \widetilde{\Delta} \tag{12}$$

The control input is redesigned as

$$u = \frac{1}{g}(-\overline{f} - \hat{\Delta} + u_s) \tag{13}$$

Then, Equation (12) is converted as

$$\dot{\sigma} = u_s + \widetilde{\Delta} \tag{14}$$

For Equation (14), the control law Equation (11) can be used. The standard second-order SMC has a good performance to deal with strong disturbances near the origin. Yet, its ability to handle disturbances far from the origin is not ideal. Linear algorithms can easily handle strong disturbances far from the origin. Thus, Equation (11) is improved by combining the advantages of the linear algorithm and the STC algorithm. The improved fast SOSM controller is presented as

$$\begin{cases} u_s = -k_1|\sigma|^{1/2} sign(\sigma) - k_2\sigma + u_1 \\ u_1 = -k_3 sign(\sigma) - k_4\sigma \end{cases} \tag{15}$$

The proof for stability and finite-time convergence can be found in [38], in which the pure mathematics model is studied.

In Equation (13), $\hat{\Delta}$ is unknown. Next, we will provide a detailed description about how to obtain the observed value.

The total disturbances value Δ in Equation (8) is expanded into a new state variable h; then,

$$\begin{cases} \dot{\sigma} = f + gu + h \\ \dot{h} = \xi(t) \end{cases} \tag{16}$$

where $\xi(t)$ is the derivative of h. Define the observed value $\hat{\sigma}$ of σ as Z_1 and the observed value $\hat{h}$ of h as Z_2. The sliding mode observer is designed as

$$\begin{cases} e_1 = Z_1 - \sigma \\ \dot{Z}_1 = f + gu + Z_2 - \alpha_1|e_1|^{1/2} sign(e_1) \\ \dot{Z}_2 = -\alpha_2 \mathrm{sign}(\mathrm{e}_1) \end{cases} \tag{17}$$

where α_1 and α_2 are the observer gains. Define the observer error dynamics $e_1 = Z_1 - \sigma$, $e_2 = Z_2 - h$, then the observer error can be expressed as

$$\begin{cases} \dot{e}_1 = -\alpha_1|e_1|^{1/2} sign(e_1) + e_2 \\ \dot{e}_2 = -\alpha_2 sign(e_1) + \chi_1 \end{cases} \tag{18}$$

where $\chi_1 = -\xi(t)$.

The values of gains α_1 and α_2 are dependent on N, which is hard to obtain in the FOWT system. To cope with this difficulty, barrier function-based SMC [39,40] is deeply analyzed and an adaptive super-twisting SOSM observer is proposed. Define $\alpha_1 = L$ and $\alpha_2 = L^2$, then Equation (17) becomes

$$\begin{cases} \dot{e}_1 = -L|e_1|^{1/2} sign(e_1) + e_2 \\ \dot{e}_2 = -L^2 sign(e_1) + \chi_1 \end{cases} \tag{19}$$

$L(t, e_1)$ is the adaptive gain, which is defined as

$$L(t, e_1) = \begin{cases} q(t) = M_1 t + M_0, & 0 \le t < t_1 \\ L_B(e_1) = \frac{\sqrt{\varepsilon} a}{(\varepsilon - |e_1|)^{1/2}}, & t \ge t_1 \end{cases} \tag{20}$$

where M_1 and M_0 are arbitrary constants, a is a positive parameter, and ε is a provided fixed value ($\varepsilon > 0$).

t_1 is the time required for $|e_1|$ to reach $\varepsilon/2$. For all $t \ge t_1$,$|e_1| < \varepsilon$ is true. This remark will be proved in two steps. The first step is to prove that there is a finite time t_1 such that e_1 in Equation (19) satisfies $e_1 \le \varepsilon/2$.

To assume $|e_1(0)| > \varepsilon/2$ and according to Equation (20), the variable gain is $q(t) = M_1 t + M_0$ as long as $|e_1| > \varepsilon/2$. At the same time, the right side of Equation (19) is sublinear relative to (e_1, e_2). This dynamic interval is defined by $H(e_1(0))$ and its form is $[0, T_0]$. To complete the proof by contradiction, it is sufficient to prove that T_0 is the required time t_1.

It is assumed that $|e_1| > \varepsilon$ on $H(e_1(0))$ and e_1 is positive. From the second equation in Equation (19), it can be obtained as

$$-q^2(t) - N \le \dot{e}_2 \le -q^2(t) + N \tag{21}$$

It can be easily found that $H(e_1(0)) = [0, \infty)$. e_2 becomes and remains negative in finite time. From the first equation of Equation (19),

$$\dot{e}_1 \le -q(t)|e_1|^{1/2} sign(e_1) \tag{22}$$

Thus, the sliding surface σ converges to zero in finite time, which is contrary to the previous assumption that $|e_1| > \varepsilon$ on $H(e_1(0))$.

The second step is to prove that for all $t \ge t_1$, $|e_1| < \varepsilon$ holds, considering variable transformation $x = (x_1, x_2)$, where $x_1 = L_B^2 \cdot e_1$ and $x_2 = e_2$. Then, it can be written as

$$\begin{cases} \dot{x}_1 = 2\frac{\dot{L}_B}{L_B} \cdot x_1 + L_B^2 \cdot \dot{e}_1 \\ \dot{x}_2 = \dot{e}_2 \end{cases} \tag{23}$$

since

$$\dot{L}_B = \frac{0.5a\sqrt{\varepsilon}(\varepsilon - |e_1|)^{-1/2}\dot{e}_1 sign(e_1)}{(\varepsilon - |e_1|)} \tag{24}$$

such that $|x_1(t_1)| \le a^2\varepsilon$ is satisfied, and the term $\frac{\dot{L}_B}{L_B}$ can be written as

$$\frac{\dot{L}_B}{L_B} = 0.5\frac{\dot{e}_1 sign(e_1)}{(\varepsilon - |e_1|)} = Y L_B^2 \dot{e}_1 sign(e_1) \tag{25}$$

where $Y = \frac{1}{2a^2\varepsilon}$. Substituting Equations (25) and (19) into Equation (23), then:

$$\begin{cases} \frac{\dot{x}_1}{1+2Y|x_1|} = L_B^2(-|x_1|^{1/2} sign(x_1) + x_2) \\ \dot{x}_2 = -L_B^2 sign(x_1) + \chi_1 \end{cases} \tag{26}$$

Define $\eta(t_1) = 0$ and $d\eta = L_B^2 dt$, and use $'$ to denote the derivative with respect to η. Then, Equation (26) can be rewritten as

$$\begin{cases} \frac{x'_1}{1+2Y|x_1|} = -|x_1|^{1/2} sign(x_1) + x_2 \\ x'_2 = -sign(x_1) + \frac{\chi_1}{L_B^2} \end{cases} \tag{27}$$

The second equation of Equation (27) shows that x'_2 is bounded. So, x_2 has a linear growth on $H(e_1(0))$ at most. It can be found that the time derivative of the positive function $\ln(1 + 2Y|x_1|)$ is upper-bounded by a function with linear growth on $H(e_1(0))$ from the first equation of Equation (27). Thus, it can be easily found that $H(e_1(0)) = [0, \infty)$. QED□

In summary, the new composite super-twisting sliding mode (CSTSM) scheme proposed in this paper is shown in Figure 2. An integral sliding mode surface was designed based on the error between the reference rotor speed and the actual rotor speed. The fast SOSM control law u_s is constructed based on the sliding mode surface. The adaptive observer for which adaptive gain is produced with the help of barrier function is designed. The designed control law (15) and observer (17), combined with the feedback control, produce the required pitch angle.

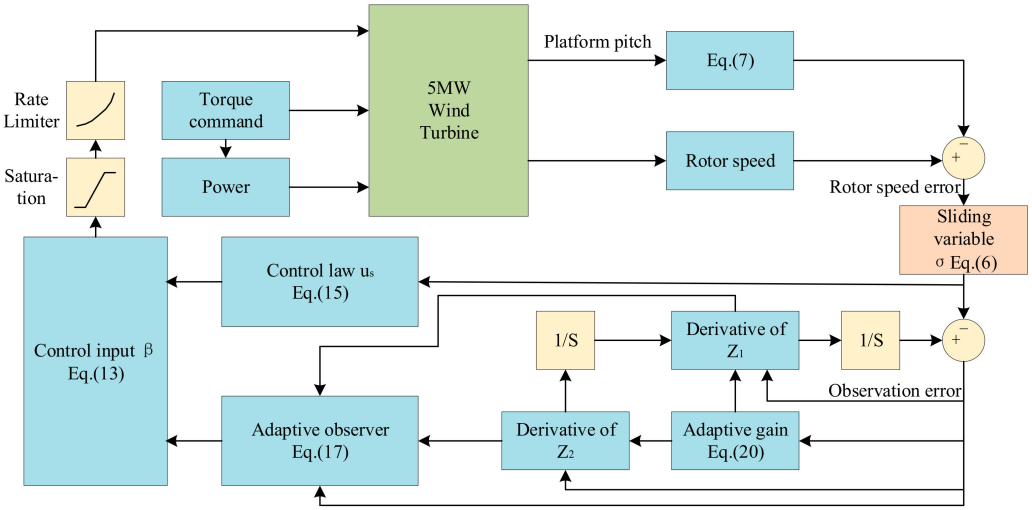

Figure 2. The CSTSM control scheme.

To compare control performance, the standard super-twisting sliding mode (SSTSM) control and PI control schemes are also designed. The SSTSM control law is

$$\begin{cases} u_{STC} = -k_5|\sigma|^{1/2} sign(\sigma) + u_C \\ u_C = -k_6 sign(\sigma) \end{cases} \tag{28}$$

where k_5 and k_6 are the control gains.

The PI control scheme is designed as:

$$u_{pi} = K_p(\omega - \omega_r) + K_i \int_0^\tau (\omega - \omega_r) d\tau \tag{29}$$

where K_p and K_i are the proportional and integral coefficients, respectively.

4. Simulation Results and Discussion

The simulation experiment was conducted on the 5 MW ITIBige4 FOWT, and the proposed controller and observer are developed in the MATLAB/Simulink environment. The simulation runtime was set to 600 s. All 24 degrees of freedom were enabled in FAST, and wind data were generated using the software Turbsim v2.00. The wind turbine parameters are shown in Table 2 [41]; Figure 3 is the simulink diagram of the proposed scheme.

Table 2. Main parameters of the FOWT.

Parameter	Value
Number of Blades	3
Rated Power	5 MW
Rotor Diameter	126 m
Hub Height	90 m
Rated Rotor Speed	12.1 rpm
Rated Wind Speed	11.4 m/s
Rotor Mass	110,000 kg
Nacelle Mass	240,000 kg
Tower Mass	347,460 kg
Generator inertia	534.116 kg·m^2
Nacelle inertia	2607.89 × 10^3 kg·m^2
Hub inertia	115.926 × 10^3 kg·m^2

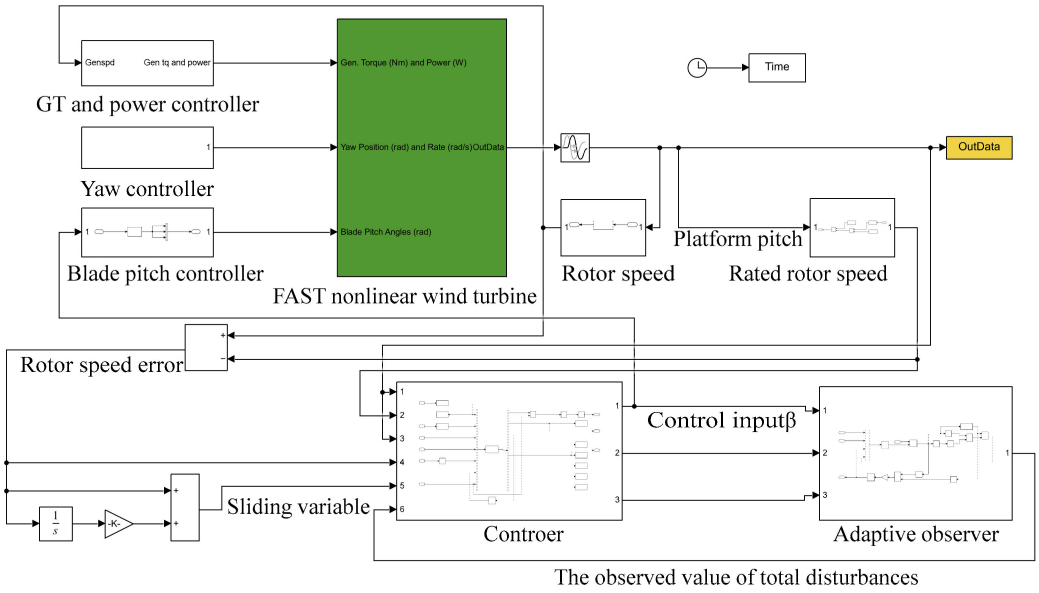

Figure 3. Simulink diagram of CSTSM.

Due to the physical limitations of the FOWT, the constraints of the pitch angle and its rate of change are $\beta \in [0°, 90°]$, and $\dot{\beta} \in [-8, 8]$ (°)/s. Two wind and wave conditions are shown in Table 3, and their respective variation is shown in Figure 4. This paper compared the performances of PI control, SSTSM control, and the CSTSM control. The fatigue loads on blades and tower were analyzed by the damage equivalent load (DEL) of MLife [42]. The DEL is obtained with a life of 20 years and a frequency of 1 Hz.

Table 3. Environmental conditions.

Case	Wind Speed (m/s)	Turbulence Intensity (%)	Significant Wave Height (m)	Peak Spectral Period (s)
Case 1	18	16.98	3.5	10.5
Case 2	20	16.48	5	12.5

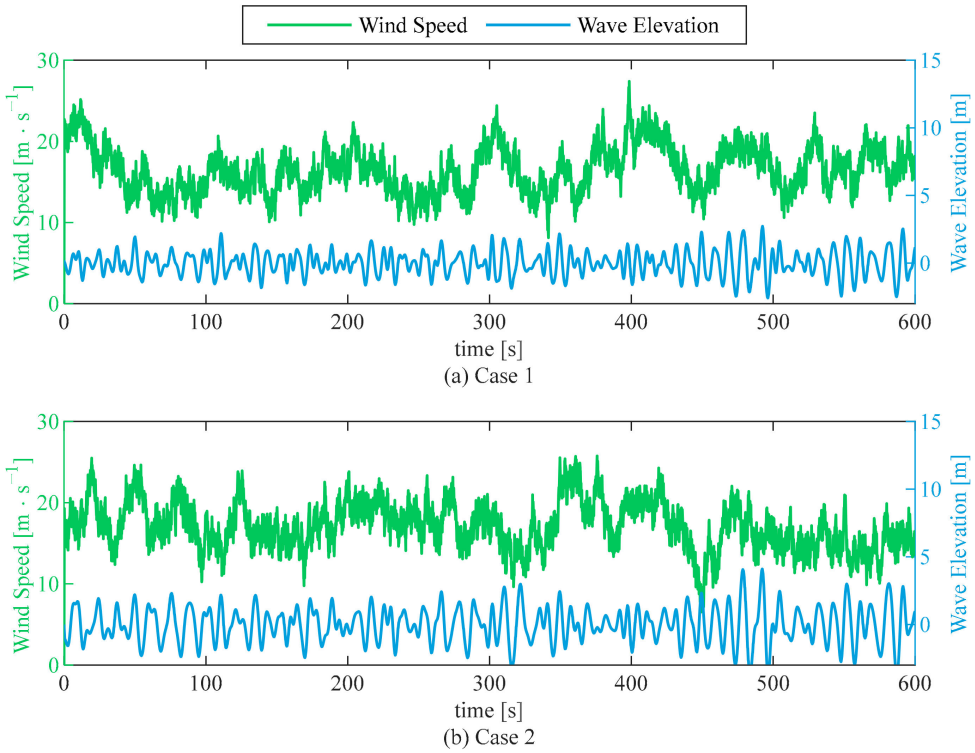

Figure 4. Environmental conditions for Case 1 and Case 2.

The control parameters of the CSTSM were selected as $k_1 = 1$, $k_2 = 2$, $k_3 = 0.23$, $k_4 = 0.01$, $\varepsilon = 0.1$, $M_1 = 0.3$, and $M_0 = 0.01$. The comparative control scheme SSTSM parameters were designed as $k_5 = 1.06$, and $k_6 = 0.3$, and the PI control parameters were designed as $K_p = 0.1$, and $K_i = 0.02$.

4.1. Time Domain Analysis of Power and Platform Motion

The root mean square (RMS) of power error and platform motion angular velocity are used to compare the control performance of the three schemes in two environments. As shown in Figure 5, compared with the PI scheme, the SSTSM scheme and the CSTSM scheme play a better role in stabilizing power. In Case 1, the platform roll under the CSTSM scheme is reduced by 13% and 4%, and pitch is reduced by 16% and 3%, respectively, compared with that under PI control scheme and SSTSM scheme. In Case 2, the roll is reduced by 9% and 15%, and the pitch is reduced by 7% and 1%, respectively. In summary, the effect under the CSTSM scheme is better than that under the PI control scheme and SSTSM scheme, and the CSTSM scheme has better adaptability to the external environment. Figure 6 shows the responses of rotor speed, power and platform motion angular velocity after the three schemes are applied, respectively, in two cases.

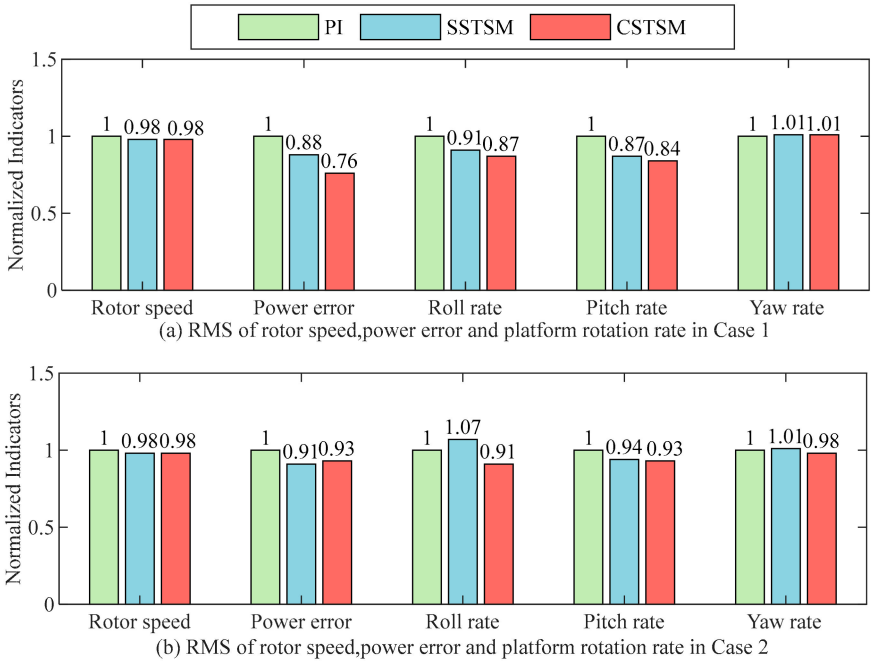

Figure 5. Normalized RMS values under the three schemes in Case 1 and Case 2.

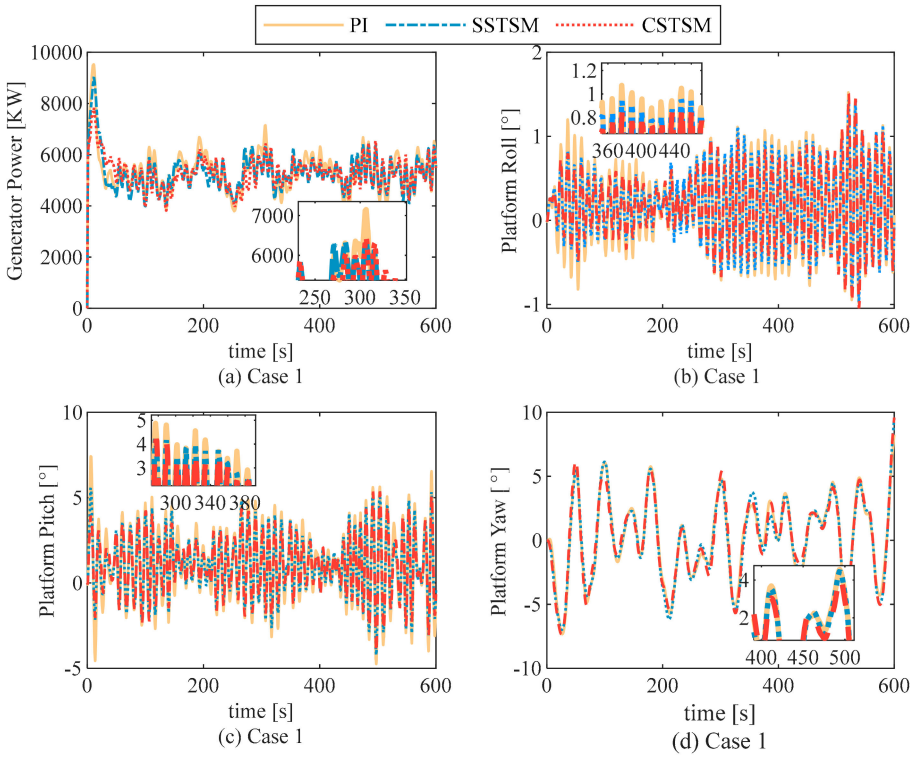

Figure 6. *Cont.*

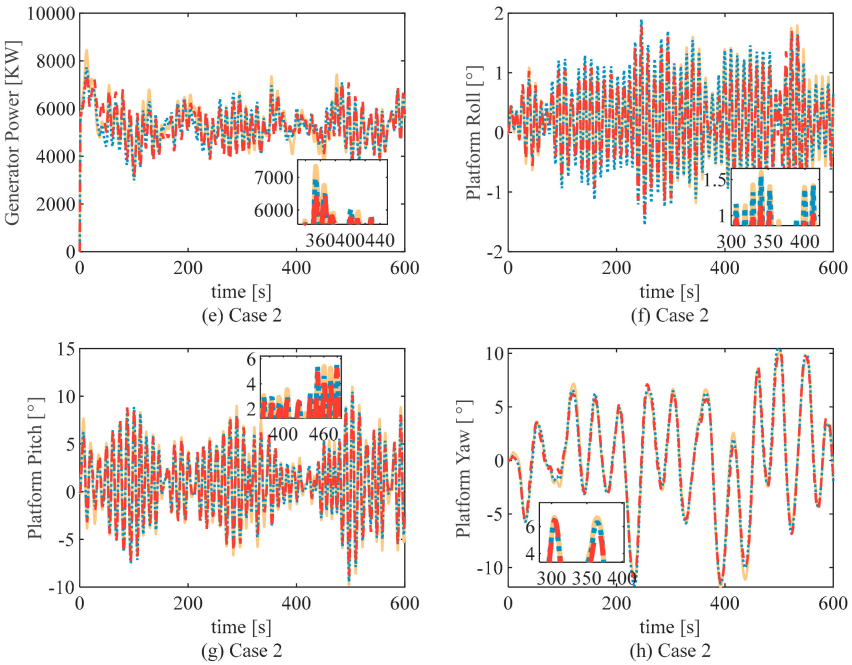

Figure 6. Power and platform motion response under Case 1 and Case 2.

4.2. Formatting of Mathematical Components

In this section, power spectral density (PSD) analysis is conducted on the output power and platform motion of the FOWT. The frequency response curves of wind speed and wave height under the two cases are presented in Figure 7. As shown in Figure 7, following the initial state, the wind speed exhibits maximum energy around 0.015 Hz in Case 1; the primary frequency range for wave height lies between 0.095 and 0.42 Hz. For Case 2, the maximum energy occurs at approximately 0.01 Hz, and the primary frequency range for wave height spans from 0.075 to 0.36 Hz. Figure 8 illustrates the output power in the low-frequency range, alongside the response curves of platform roll and pitch under the influence of three control schemes across two cases. As discernible from Figure 8a,d, regarding FOWT output power, the CSTSM control scheme exhibits superior control efficacy compared to the PI control scheme at peak wind speed energy. As can be observed from Figure 8b,c,e,f, the CSTSM control scheme can still maintain a good inhibition effect on platform roll and pitch despite changes in the environment.

4.3. Tower and Blade Load Analysis

In Figure 9, the DEL normalization values of the tower and blade roots under the three schemes are compared. In Case 1, for the tower top pitch moment, load reductions of 9% and 3% are achievable compared with that under the PI control scheme and SSTSM scheme. For the tower top yaw moment, load reductions of 7% and 1% are achievable. Both the SSTSM scheme and the CSTSM scheme reduce the overall DEL normalized values of the tower base moment and the tower top moment, and the CSTSM scheme has a better effect on load suppression than the SSTSM scheme. When the external environment is changed, as shown in Case 2, for the tower top pitch moment, load reductions of 7% and 2% are achievable compared with that under the PI control scheme and SSTSM scheme. For the tower top yaw moment, load reductions of 3% and 6% are achievable. The CSTSM scheme can still effectively reduce the overall DEL normalized values of tower base moment and tower top moment compared with SSTSM scheme. It can be seen that the CSTSM scheme has stronger adaptability to the environment in terms of tower load suppression. Figure 10a,b show the time domain response curves of the blade pitch angle for the three control schemes applied to the floating wind turbine under Case 1 and Case 2. It can be observed from the diagrams when compared with the PI control scheme that the blade

pitch angle of both the SSTSM scheme and the CSTSM scheme exhibits bigger fluctuation. Figure 10c,d display the pitch angle frequency domain response curves of the three control schemes for the floating wind turbine under Case 1 and Case 2. It is evident from the diagrams that in comparison with the PI control scheme, the blade pitch fluctuation energy of both the SSTSM scheme and CSTSM scheme is larger. But, blade pitch saturation and change rate limit are considered in the simulation, and the DEL value of the inside and outside plane moment at the blade root does not increase much, that is, the influence of blade actuator fluctuation on blade fatigue life is within a reasonable range.

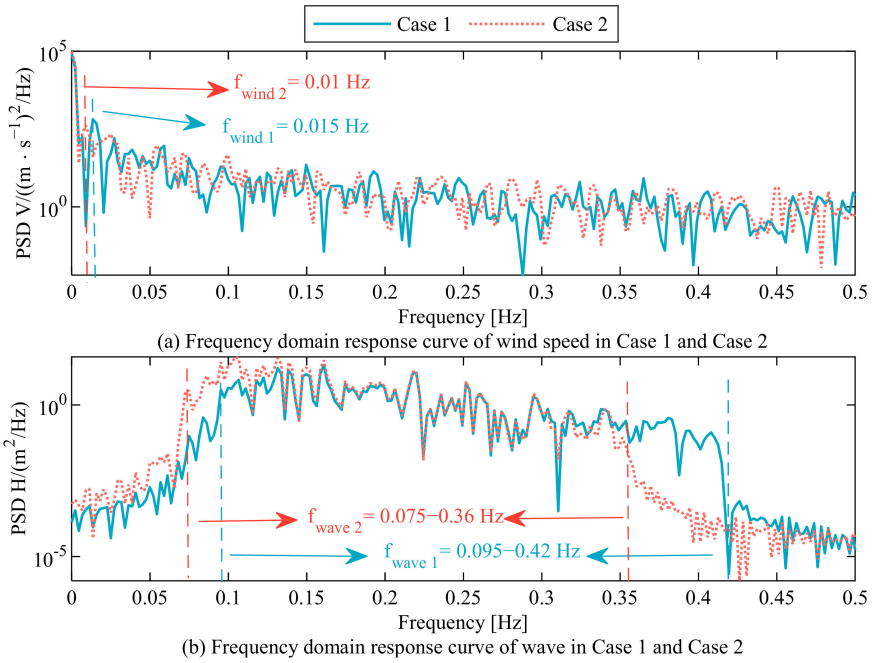

Figure 7. Frequency domain response of wind speed and wave in Case 1 and Case 2.

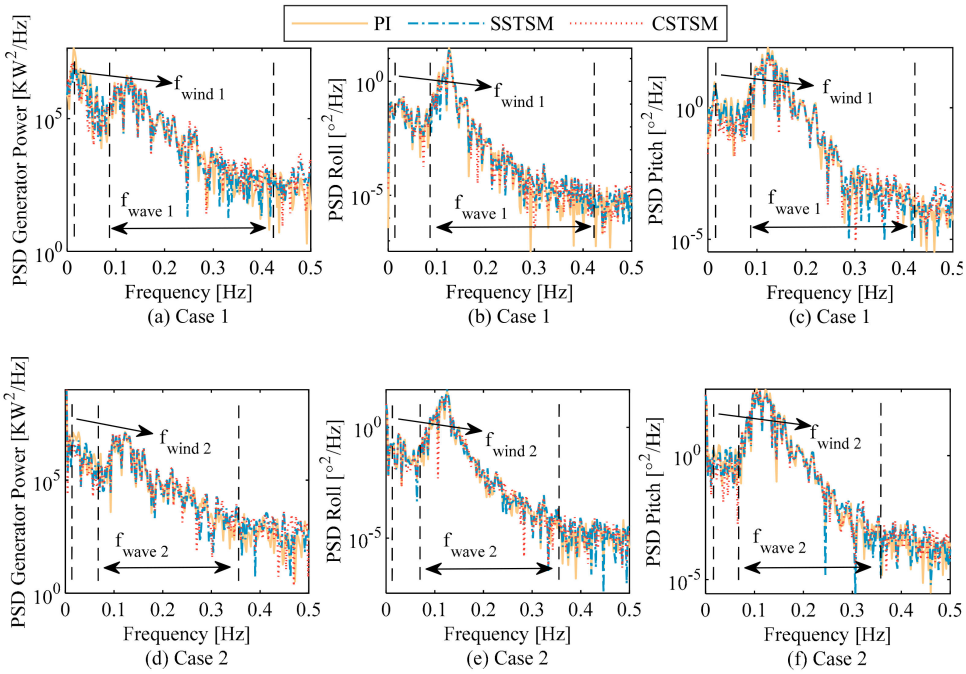

Figure 8. Frequency domain response of power and platform in Case 1 and Case 2.

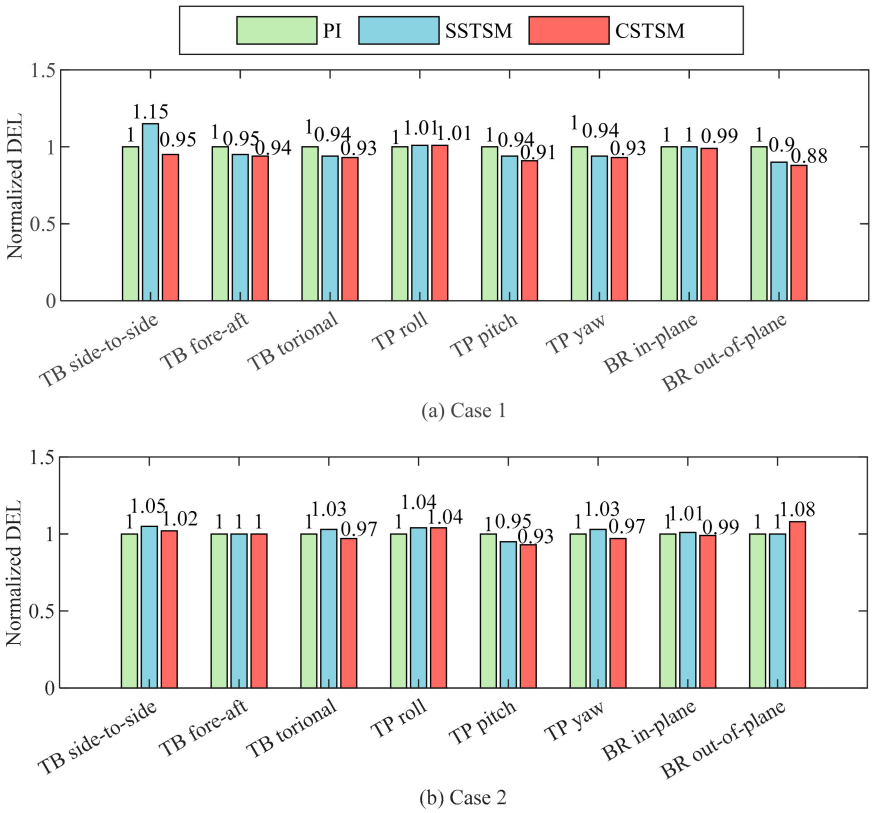

Figure 9. Normalized DEL values of tower base moments, tower top moments and blade root moments obtained with the three schemes in Case 1 and Case 2.

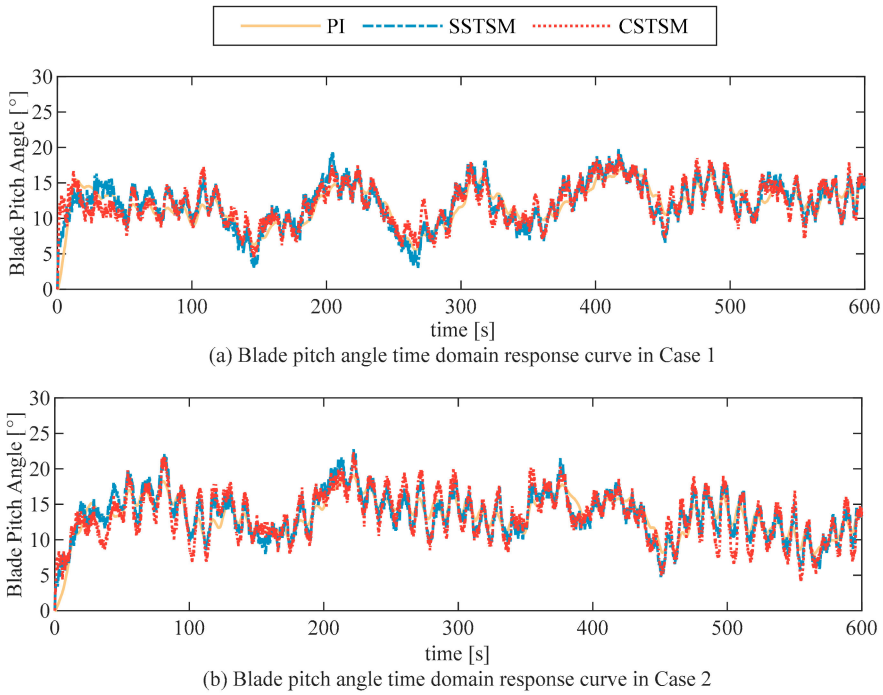

Figure 10. *Cont.*

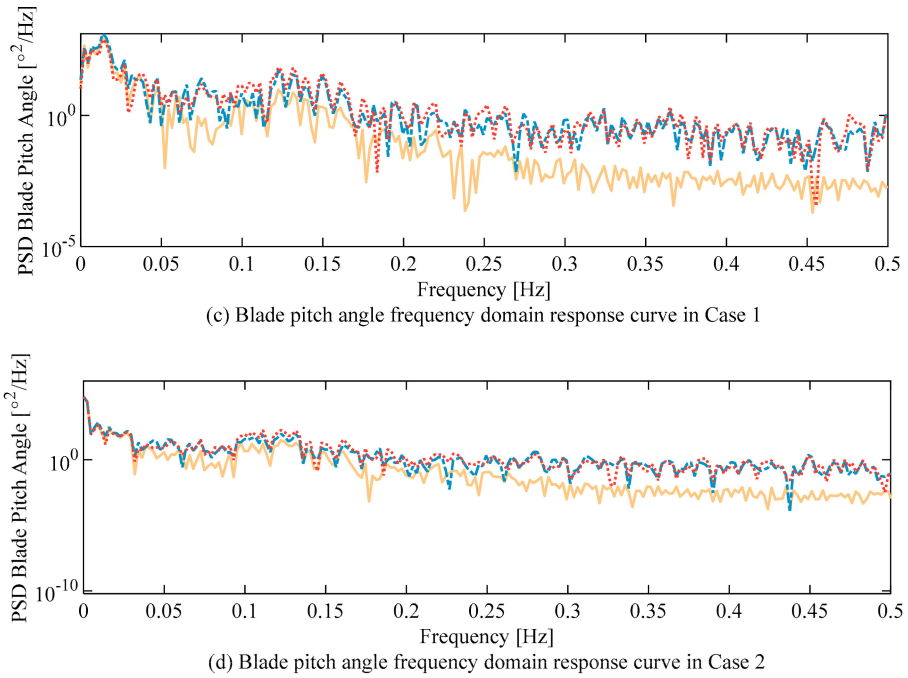

Figure 10. Blade pitch angle obtained with the three schemes in Case 1 and Case 2.

4.4. Observer Performance

Simulation results prove that the CSTSM scheme can effectively reduce the fatigue load of the tower. In addition, this scheme can observe and compensate for disturbances and uncertainties. As shown in Figure 11a,c, the observer gains can be dynamically adjusted with disturbances, which greatly reduces parameter adjustment workload and control gains. The observed sliding mode surface error is shown in Figure 11b,d. The observer can still maintain good performance after the external environment is changed.

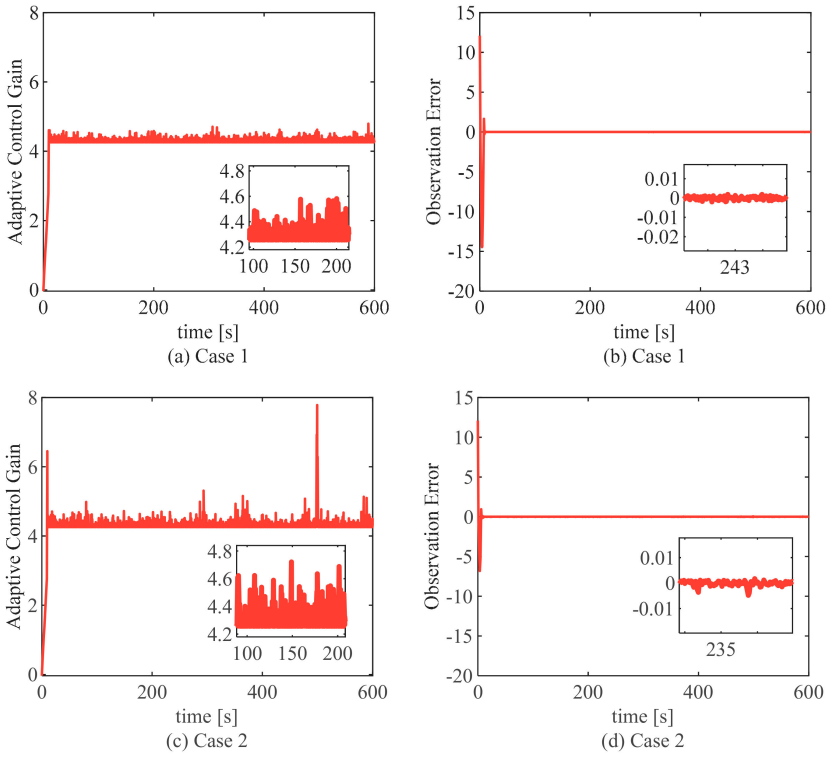

Figure 11. Adaptive control gains and observation error in Case 1 and Case 2.

5. Conclusions

In this paper, a new composite blade pitch control scheme based on a fast SOSM controller and an adaptive super-twisting sliding mode extended state observer is proposed. A new adaptive super-twisting extended state observer is constructed to achieve total disturbance observation and compensated to reduce the controller gains. Compared with the PI control scheme and SSTSM scheme, in Case 1, the platform roll under the proposed CSTSM scheme is reduced by 13% and 4%, and pitch is reduced by 16% and 3%. Respectively, in Case 2, the roll is reduced by 9% and 15%, and pitch is reduced by 7% and 1%. For the tower top pitch moment, load reductions of 7% and 2% or more are achievable compared with those under the PI control scheme and SSTSM scheme. For the tower top yaw moment, load reductions of 3% and 1% or more are achievable compared with the PI control scheme and SSTSM scheme. Therefore, the proposed CSTSM scheme is more effective in restraining floating platform motion, stabilizing output power and restraining tower load, and has stronger adaptability to the environment. It should be noted that the proposed CSTSM scheme is carried out under simulation conditions, yet, the FOWT faces a more complex operating environment and unknown factors in actual operation. In future work, further optimization of the algorithm and its application in practice will be a breakthrough in this field.

Author Contributions: Conceptualization, W.Y. and Y.H.; data curation, W.Y. and R.M.; formal analysis, Y.H. and G.Y.; methodology, W.Y. and Y.H.; project administration, Y.H.; resources, W.Y.; supervision, R.M. and M.H.; validation, R.M.; writing—original draft, W.Y. and R.M.; writing—review and editing, W.Y., G.Y. and Y.H. All authors have read and agreed to the published version of the manuscript.

Funding: This research was funded by Shandong Provincial Natural Science Foundation under Grant ZR2023MF034; National Natural Science Foundation of China under Grant 61803230; and Project of Shandong Province College Youth Innovation Technology Support Program under Grant 2019KJN023.

Institutional Review Board Statement: Not applicable.

Informed Consent Statement: Not applicable.

Data Availability Statement: Data are contained within the article.

Conflicts of Interest: The authors declare no conflict of interest.

References

1. Jung, C.; Schindler, D. Efficiency and effectiveness of global onshore wind energy utilization. *Energy Convers. Manag.* **2023**, *280*, 116788. [CrossRef]
2. Tian, H.; Soltani, M.N.; Nielsen, M.E. Review of floating wind turbine damping technology. *Ocean Eng.* **2023**, *278*, 114365. [CrossRef]
3. Micallef, D.; Rezaeiha, A. Floating offshore wind turbine aerodynamics: Trends and future challenges. *Renew. Sustain. Energy Rev.* **2021**, *152*, 111696. [CrossRef]
4. Shah, S.A.A.; Gao, B.; Ahmad, I.; Ullah, H.; Ahmed, N.; Saeed, A. Adaptive Backstepping Integral Sliding Mode Control for 5DOF Barge-Type OFWT under Output Constraint. *J. Mar. Sci. Eng.* **2023**, *11*, 492. [CrossRef]
5. Shah, K.A.; Meng, F.; Li, Y.; Nagamune, R.; Zhou, Y.; Ren, Z.; Jiang, Z. A synthesis of feasible control methods for floating offshore wind turbine system dynamics. *Renew. Sustain. Energy Rev.* **2021**, *151*, 111525. [CrossRef]
6. Ha, K.; Truong, H.V.A.; Dang, T.D.; Ahn, K.K. Recent control technologies for floating offshore wind energy system: A review. *Int. J. Precis. Eng. Manuf.-Green Technol.* **2021**, *8*, 281–301. [CrossRef]
7. Zhang, M.; Li, X.; Tong, J.; Xu, J. Load control of floating wind turbine on a Tension-Leg-Platform subject to extreme wind condition. *Renew. Energy* **2020**, *151*, 993–1007. [CrossRef]
8. Park, G.; Oh, K.-Y.; Nam, W. Bilinear tuned mass damper for spar-type floating wind turbines. *Ocean. Eng.* **2022**, *261*, 112081. [CrossRef]
9. Clement, C.; Kosleck, S.; Lie, T. Investigation of viscous damping effect on the coupled dynamic response of a hybrid floating platform concept for offshore wind turbines. *Ocean. Eng.* **2021**, *225*, 108836. [CrossRef]
10. Lackner, M.A.; Rotea, M.A. Passive structural control of offshore wind turbines. *Wind. Energy* **2011**, *14*, 373–388. [CrossRef]

11. Stewart, G.; Lackner, M. Offshore wind turbine load reduction employing optimal passive tuned mass damping systems. *IEEE Trans. Control. Syst. Technol.* **2013**, *21*, 1090–1104. [CrossRef]
12. Sarkar, S.; Fitzgerald, B. Vibration control of spar-type floating offshore wind turbine towers using a tuned mass-damper-inerter. *Struct. Control Health Monit.* **2020**, *27*, e2471. [CrossRef]
13. Javier, L.; Eider, R.; Josu, J.; Santiago, A. Review of Control Technologies for Floating Offshore Wind turbines. *Renew. Sustain. Energy Rev.* **2022**, *167*, 112787.
14. Larsen, T.J.; Hanson, T.D. A method to avoid negative damped low frequent tower vibrations for a floating, pitch controlled wind turbine. In *Proceedings of the Journal of Physics: Conference Series*; IOP Publishing: Bristol, UK, 2007; p. 12073.
15. Zhang, Y.; Yang, X.; Liu, S. Data-driven predictive control for floating offshore wind turbines based on deep learning and multi-objective optimization. *Ocean. Eng.* **2022**, *266*, 112820. [CrossRef]
16. Wakui, T.; Yoshimura, M.; Yokoyama, R. Multiple-feedback control of power output and platform pitching motion for a floating offshore wind turbine-generator system. *Energy* **2017**, *141*, 563–578. [CrossRef]
17. Radaideh, A.; Bodoor, M.M.; Al-Quraan, A. Active and reactive power control for wind turbines based DFIG using LQR controller with optimal gain-scheduling. *J. Electr. Comput. Eng.* **2021**, *2021*, 1–19. [CrossRef]
18. Sarkar, S.; Chen, L.; Fitzgerald, B.; Basu, B. Multi-resolution wavelet pitch controller for spar-type floating offshore wind turbines including wave-current interactions. *J. Sound Vib.* **2020**, *470*, 115170. [CrossRef]
19. Yang, B.; Yu, T.; Shu, H.; Dong, J.; Jiang, L. Robust sliding-mode control of wind energy conversion systems for optimal power extraction via nonlinear perturbation observers. *Appl. Energy* **2018**, *210*, 711–723. [CrossRef]
20. Kelkoul, B.; Boumediene, A. Stability analysis and study between classical sliding mode control (SMC) and super twisting algorithm (STA) for doubly fed induction generator (DFIG) under wind turbine. *Energy* **2021**, *214*, 118871. [CrossRef]
21. Shah, S.A.A.; Gao, B.; Ahmed, N.; Liu, C. Advanced robust control techniques for the stabilization of translational oscillator with rotational actuator based barge-type OFWT. *Proc. Inst. Mech. Eng. Part M J. Eng. Marit. Environ.* **2021**, *235*, 327–343. [CrossRef]
22. Han, Y.; Liu, X. Continuous higher-order sliding mode control with time-varying gain for a class of uncertain nonlinear systems. *ISA Trans.* **2016**, *62*, 193–201. [CrossRef]
23. Liu, X.; Wang, C.; Han, Y. Second-order sliding mode control of DFIG based variable speed wind turbine for maximum power point tracking. *Acta Autom. Sin.* **2017**, *43*, 1434–1442.
24. Zhang, C.; Gutierrez, S.; Plestan, F.; de León-Morales, J. Adaptive super-twisting control of floating wind turbines with collective blade pitch control. *IFAC-Pap.* **2019**, *52*, 117–122. [CrossRef]
25. Zhang, C.; Plestan, F. Individual/collective blade pitch control of floating wind turbine based on adaptive second order sliding mode. *Ocean. Eng.* **2021**, *228*, 108897. [CrossRef]
26. Gutierrez, S.V.; Zhang, C.; de Leon-Morales, J.; Plestan, F. A simplified version of adaptive super twisting—Application to the control of floating wind turbine. *Control Eng. Pract.* **2022**, *125*, 105208. [CrossRef]
27. Li, S.; Han, Y.; Pan, W.; Liu, S.; Hou, M. Variable-gain higher-order sliding mode pitch control of floating offshore wind turbine. *J. Mar. Sci. Eng* **2021**, *9*, 1172. [CrossRef]
28. Ali, S.A.; Langlois, N. Sliding mode control for diesel engine air path subject to matched and unmatched disturbances using extended state observer. *Math. Probl. Eng.* **2013**, *2013*, 712723. [CrossRef]
29. Guermouche, M.; Ali, S.A.; Langlois, N. Super-twisting algorithm for DC motor position control via disturbance observer. *IFAC-Pap.* **2015**, *48*, 43–48. [CrossRef]
30. Mohamed, G.; Sofiane, A.A.; Nicolas, L. Adaptive super twisting extended state observer based sliding mode control for diesel engine air path subject to matched and unmatched disturbance. *Math. Comput. Simul.* **2018**, *151*, 111–130. [CrossRef]
31. Zhao, L.; Zheng, C.; Wang, Y.; Liu, B. A finite-time control for a pneumatic cylinder servo system based on a super-twisting extended state observer. *IEEE Trans. Syst. Man Cybern. Syst.* **2019**, *51*, 1164–1173. [CrossRef]
32. Yang, Y.; Yan, Y.; Xu, X.; Gong, B. Super-twisting algorithm with fast super-twisting disturbance observer for steer-by-wire vehicles. *Proc. Inst. Mech. Eng. Part D J. Automob. Eng.* **2021**, *235*, 2324–2340. [CrossRef]
33. Liu, Q.-S.; Miao, W.-P.; Yue, M.-N.; Li, C.; Wang, B.; Ding, Q. Dynamic response of offshore wind turbine on 3× 3 barge array floating platform under extreme sea conditions. *China Ocean. Eng.* **2021**, *35*, 186–200. [CrossRef]
34. Jonkman, J.M.; Buhl, M.L. *FAST User's Guide*; National Renewable Energy Laboratory: Golden, CO, USA, 2005; Volume 365.
35. Colombo, L.; Corradini, M.L.; Ippoliti, G.; Orlando, G. Pitch angle control of a wind turbine operating above the rated wind speed: A sliding mode control approach. *ISA Trans.* **2020**, *96*, 95–102. [CrossRef] [PubMed]
36. Lackner, M.A. An investigation of variable power collective pitch control for load mitigation of floating offshore wind turbines. *Wind. Energy* **2013**, *16*, 435–444. [CrossRef]
37. Seeber, R.; Horn, M. Stability proof for a well-established super-twisting parameter setting. *Automatica* **2017**, *84*, 241–243. [CrossRef]
38. Moreno, J.A.; Osorio, M. A Lyapunov approach to second-order sliding mode controllers and observers. In Proceedings of the 2008 47th IEEE Conference on Decision and Control, Cancun, Mexico, 9–11 December 2008; pp. 2856–2861.
39. Obeid, H.; Fridman, L.; Laghrouche, S.; Harmouche, M.; Golkani, M.A. Adaptation of Levant's differentiator based on barrier function. *Int. J. Control* **2018**, *91*, 2019–2027. [CrossRef]
40. Obeid, H.; Laghrouche, S.; Fridman, L.; Chitour, Y.; Harmouche, M. Barrier function-based adaptive super-twisting controller. *IEEE Trans. Autom. Control* **2020**, *65*, 4928–4933. [CrossRef]

41. Jonkman, J.; Butterfield, S.; Musial, W.; Scott, G. *Definition of a 5-MW Reference Wind Turbine for Offshore System Development*; National Renewable Energy Laboratory: Golden, CO, USA, 2009.
42. Hayman, G. *MLife Theory Manual for Version 1.00*; National Renewable Energy Laboratory: Golden, CO, USA, 2012; Volume 74, p. 106.